

# A Novel Generative Neural Approach for InSAR Joint Phase Filtering and Coherence Estimation

Subhayan Mukherjee, Aaron Zimmer, Xinyao Sun, Parwant Ghuman, Irene Cheng *Senior Member, IEEE*

**Abstract**—Earth’s physical properties like atmosphere, topography and ground instability can be determined by differencing billions of phase measurements (pixels) in subsequent matching Interferometric Synthetic Aperture Radar (InSAR) images. Quality (coherence) of each pixel can vary from perfect information (1) to complete noise (0), which needs to be quantified, alongside filtering information-bearing pixels. Phase filtering is thus critical to InSAR’s Digital Elevation Model (DEM) production pipeline, as it removes spatial inconsistencies (residues), immensely improving the subsequent unwrapping. Recent explosion in quantity of available InSAR data can facilitate Wide Area Monitoring (WAM) over several geographical regions, if effective and efficient automated processing can obviate manual quality-control. Advances in parallel computing architectures and Convolutional Neural Networks (CNNs) which thrive on them to rival human performance on visual pattern recognition makes this approach ideal for InSAR phase filtering for WAM, but remains largely unexplored. We propose “GenInSAR”, a CNN-based generative model for joint phase filtering and coherence estimation. We use satellite and simulated InSAR images to show overall superior performance of GenInSAR over five algorithms qualitatively, and quantitatively using Phase and Coherence Root-Mean-Squared-Error, Residue Reduction Percentage, and Phase Cosine Error.

**Index Terms**—Synthetic Aperture Radar, Neural Networks, Image Filtering, Radar Interferometry, Unsupervised Learning.

## I. INTRODUCTION

**I**NSAR or Interferometric Synthetic Aperture Radar is an emerging, highly successful remote sensing technique for measuring several geophysical quantities like surface deformation [1]. It is based on generating an interferogram as the complex difference of two SAR acquisitions of the same scene from slightly different view angles. The wrapped interferometric phase is then unwrapped to subsequently produce a Digital Elevation Model (DEM). However, several decorrelation factors create strong phase noise, affecting unwrapping and DEM accuracy [2]. Thus phase filtering is preferred, even when it results in some decrease in resolution and increase in spatial correlation [3] and we need filters adapted to enhance phase rather than amplitude [4]. Filtering the real and imaginary parts of the complex phase in its wrapped form [5], [6] can avoid blurring edges, whereas unwrapping before filtering increases computation and potentially decreases accuracy [1]. Due to the non-stationary nature of InSAR signal, simple boxcar

averaging and non-adaptive filtering methods tend to distort the phase [3], [5]. Methods that adapt their parameters based on, e.g. local phase quality (coherence) yield better results, as coherence is related to phase noise deviation [2], [6]. Early spatial methods like Lee [7] and frequency based methods like Goldstein [8] and their numerous improvements [9], [10], [11], [12], [13], [14] adapt to the local fringe direction and/or local noise. Frequency based methods gradually evolved into the wavelet domain [15], [16], [17] to simplify the separation of true phase from noise [2] but struggled to filter dense fringes, whereas spatial methods in general sacrificed spatial resolution [18]. The additive noise model of interferometric phase [7] inspired early filtering methods which assumed a stationary and consistent phase over the filtering window, but real-world challenges of strong topographic change and restrictions imposed on window size motivated more recent non-linear models [19] and per-pixel filtering [20]. Recent advances in parallel computing architectures have motivated parallelism in the InSAR processing pipeline [21], which is critical to our proposed phase filtering method (“GenInSAR”) for InSAR-based Wide Area Monitoring (WAM) across geographical regions on petabytes of data. Thus, we use a Convolutional Neural Network (CNN) architecture which seamlessly integrates with modern parallel architectures built on Graphics Processing Units (GPUs) and rival human performance on pattern recognition tasks. CNNs’ use in InSAR phase processing in particular has been limited to volcano deformation monitoring [22] via transfer learning using a popular pre-trained optical image classification CNN [23], but not direct training on InSAR data. Recent CNN-based InSAR phase filtering and coherence estimation/classification [24], [25] performed training directly on InSAR data, but their filtering and coherence estimation is separated, and their “raw” coherence is generated/preprocessed using traditional methods. In contrast, GenInSAR performs joint phase filtering and coherence estimation using only a single neural network. Our approach predicts the distribution of the center pixel given only its neighborhood (patch) and is thus “embarrassingly parallel” [26]. In contrast, non-local filters [27], [28] require computing patch similarity and suffer from terrace-like DEM artefacts, over-smoothing and “rare patch” effect [29]. For similar computational concerns, we do not adopt strategies that are iterative [3], [4] (could also result in loss of detailed features [3]), multi-stage [29], [4] and require optimization during inference, e.g. via sparse coding [1].

We propose a novel InSAR phase filter inspired by Mixture Density Networks (MDN) [30]. A CNN’s convolutional layers operating on a phase patch predict the parameters of a bi-

Manuscript submitted for review on D A T E. This work was supported by NSERC Discovery Grant and DND Supplement.

S. Mukherjee, X. Sun and I. Cheng are with the Department of Computing Science, University of Alberta, Edmonton, AB T6G 2R3 Canada (e-mails: mukherje,xinyao1,locheng@ualberta.ca).

A. Zimmer and P. Ghuman are with 3vGeomatics, Vancouver, BC V5Y 0M6 Canada (e-mails: azimmer,pghuman@3vgeomatics.com).

variate Gaussian distribution (real and imaginary channel) of the center pixel. The predicted vector  $\vec{\mu}$  represents the filtered pixel. Its coherence is a function of the predicted  $\vec{\sigma}$ . This approach improves phase filtering, and being a generative model, sampling from this distribution generates new interferograms which are slight variations on the filter output, and can be utilized to improve the InSAR pipeline, as discussed later on.

## II. PROPOSED METHOD

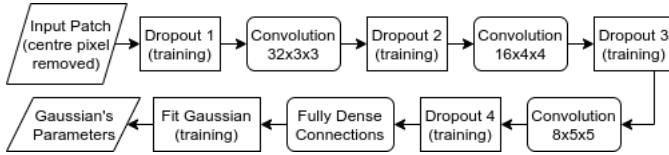


Fig. 1. Architecture of our proposed method.

The architecture of GenInSAR is shown in Fig. 1. The input to the architecture is a  $11 \times 11$  phase patch centered around the pixel to be filtered. That pixel is removed from the input patch to avoid learning the identity mapping. We can understand this more clearly in terms of the training (fitting) and testing (prediction) steps. While training, patches extracted from a fixed set of phase images (training set) are input to the model. We set 20% dropout rate [31] for the first dropout layer and 50% for the remaining ones during training to prevent over-fitting. Convolutional layers [32] of increasing filter size ( $3 \times 3$ ,  $4 \times 4$ ,  $5 \times 5$ ) and decreasing filter counts (32, 16, 8), each followed by an Exponential Linear Unit activation [33] (not shown) promote non-linear mappings. Specifically, we use depth-wise separable 2D convolutions [34] for fast computation and convergence. Finally, following MDN working principle, dense connections (weighted sums of all filter outputs) to the distribution fitting module outputs those Gaussian parameter values ( $\vec{\mu}$ ,  $\vec{\sigma}$ ) for the real and imaginary channel that make the input patch's central pixel (training target) most likely. Thus, our training is completely unsupervised, because we learn from the input data itself, without requiring its "clean" version as the training target. Negative log-likelihood cost is minimized via gradient descent back-propagation using Adam optimizer [35]. During testing, the central pixel is still removed from the input patch, but dropout and distribution fitting are not required: We predict the central pixel without any time-consuming optimization. The coherence is computed as  $\gamma = \sqrt{1 - (\sigma_{real}^2 + \sigma_{imag}^2)}$  for predicted  $\vec{\sigma} = (\sigma_{real}, \sigma_{imag})$ . Thus  $\gamma$  is more useful than many existing coherence metrics as it measures filtering efficiency, which partially depends on the spatial noise pattern (neighborhood), not just the noise underlying the center pixel.

## III. RESULTS AND DISCUSSION

We implemented GenInSAR in Keras [36] with Tensorflow-GPU backend, and compared its performance with five existing methods: Boxcar, Goldstein, NLSAR, NLSAR and the CNN-based InSAR filter mentioned earlier (hereafter referred to as "CNN-InSAR" [24]), all implemented / executed in OpenCL 1.2 on 8 GB NVIDIA 1070 GPU. In this section,

we present the qualitative and quantitative results of those experiments for real and simulated images respectively. The metrics used for quantitative analysis are Root-Mean-Square-Error (RMSE) of the InSAR phase and coherence, Residue Reduction Percentage (RRP) [3], [2], [18], and Phase Cosine Error,  $\epsilon_{cos}^{\Delta\theta}$  (Eq. 1) where  $g_i$  and  $\bar{f}_i$  denote  $i^{th}$  ground truth and complex conjugate of filtered pixels of an  $n$  pixel interferogram. Residues are phase inconsistencies emphasized by computing curl of phase differences over the range of a reduced closed integral loop of four spatially adjacent pixels [37], [18], which are non-zero if residues are present. Most residues are caused by noise. However, few arise from signal structure, like steep change in topography or heavy deformations, and those residues should be preserved during filtering. Filtering should remove all other residues to facilitate phase unwrapping. Those that cannot be removed should have low values in the filter's output coherence map; this prevents error propagation during phase difference integration by the unwrapper. Hence, filtering aims to reduce residues (high RRP) but preserve details (low Phase RMSE,  $\epsilon_{cos}^{\Delta\theta}$ ). These criteria drive our evaluations:

1) *Experiments using satellite InSAR images:* We trained GenInSAR for 100 epochs on 5 million  $11 \times 11$  patches extracted from numerous interferograms of an airport and a mining site, having resolutions  $5060 \times 4040$  and  $1000 \times 1000$  respectively, in batches of 64 patches each. We tested the model on  $1000 \times 1000$  interferograms of a different mining site, by extracting one  $11 \times 11$  patch for each pixel (at center). The interferogram edges were replicated for obtaining patches corresponding to the edge pixels. Fig. 2 shows outputs for a test interferogram using proposed and existing methods. Being a generative model, we can sample from the predicted Gaussian to generate slightly different outputs for the same input, as in Fig. 3. This can be used in InSAR machine learning for data augmentation [38], or to test InSAR processing chains by running the same chain all the way through but with slightly different interferograms to measure the variance of the outputs of the complete processing chain. This might also turn out to be a good error analysis method.

2) *Experiments using simulated InSAR images:* Our InSAR simulator can simulate ground truth interferograms with Gaussian bubbles, roads and buildings. We followed a similar training strategy as satellite InSAR images for training our model with simulated InSAR images, by adding Gaussian noise to simulated ground truth images, and inputting patches extracted from those noisy versions. For CNN-InSAR, we generated two sets of results: one using the model as-is and another by retraining it with simulated noisy images as mentioned above. For evaluating the proposed and five existing methods mentioned earlier including CNN-InSAR (as-is and retrained), we used a set of 60  $1000 \times 1000$  noisy simulated images. Fig. 4 shows the performance of all methods for a sample simulated test image. The corresponding clean (ground truth) versions of those images facilitated quantitative evaluation in terms of the three metrics mentioned earlier. Table I shows overall superior quantitative performance of proposed method against others and almost linear speedup with increasing number of GPUs, as it filters each pixel independently, based on its neighborhood.

GenInSAR almost totally reduces residues and produces far

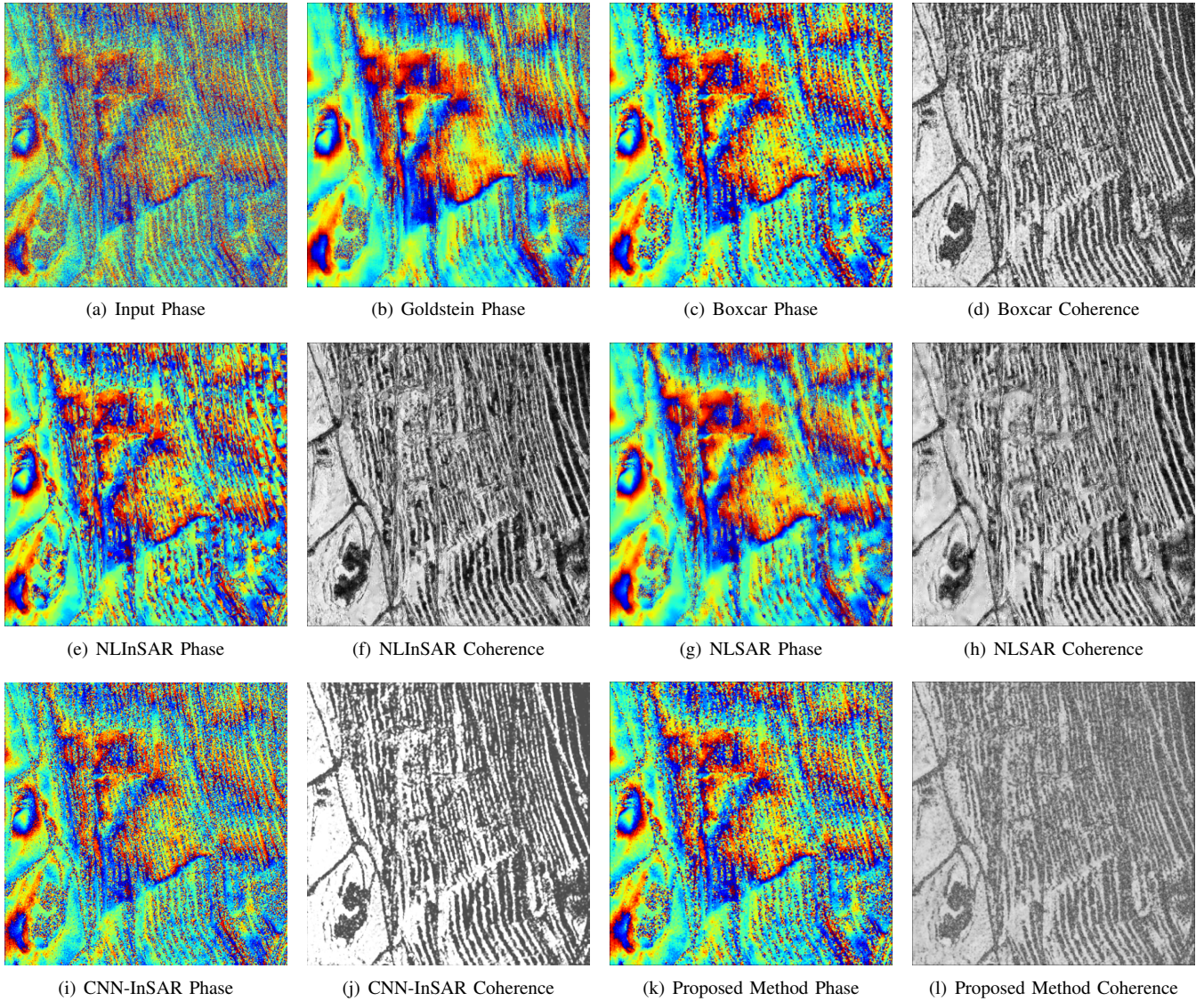


Fig. 2. Filtered phase and coherence outputs for satellite InSAR images processed by proposed and five existing methods. Visualizations for phase are coloured between  $-\pi$  (blue) to  $+\pi$  (red), and coherence between 0 (black: low) to 1 (white: high) respectively.

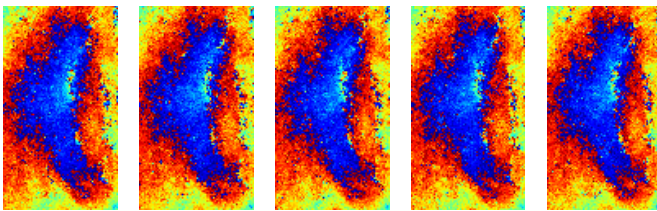


Fig. 3. Cropped interferometric phase images generated by proposed method for the same noisy input. Visualizations coloured from  $-\pi$  (blue) to  $+\pi$  (red).

less over-smoothing/artefacts around branch cuts compared to Boxcar because it’s greatest strength is (unsupervised) learning of true spatial smoothing only from noisy training data. It could potentially detect real residues better if trained more on such types of features, and an efficient implementation like those of other methods [39] could reduce it’s run time. In general, NLSAR handles residues well and avoids artefacts by

selecting neighbors with similar phase, but produces streaking correlated with low coherence bands. NLSAR (conservatively) interpolates well only over heavy noise. A final scope of future work for GenInSAR is improving the coherence function to more elegantly handle practical scenarios where the input data does not lie on the unit circle as currently,  $(\sigma_{real}^2 + \sigma_{imag}^2)$  is clipped to  $[0, 1]$ , although most values lie in that range.

$$\epsilon_{cos}^{\Delta\theta} = \frac{1}{n} \sum_{i=1}^n \frac{1}{2} (1 - \cos(\arg(g_i \bar{f}_i))) \quad (1)$$

## REFERENCES

- [1] C. Ojha, A. Fusco, and I. M. Pinto, “Interferometric sar phase denoising using proximity-based k-svd technique,” *Sensors*, vol. 19, no. 12, 2019.
- [2] Y. Wang, H. Huang, Z. Dong, and M. Wu, “Modified patch-based locally optimal wiener method for interferometric sar phase filtering,” *ISPRS Journal of Photogrammetry and Remote Sensing*, vol. 114, pp. 10 – 23, 2016.

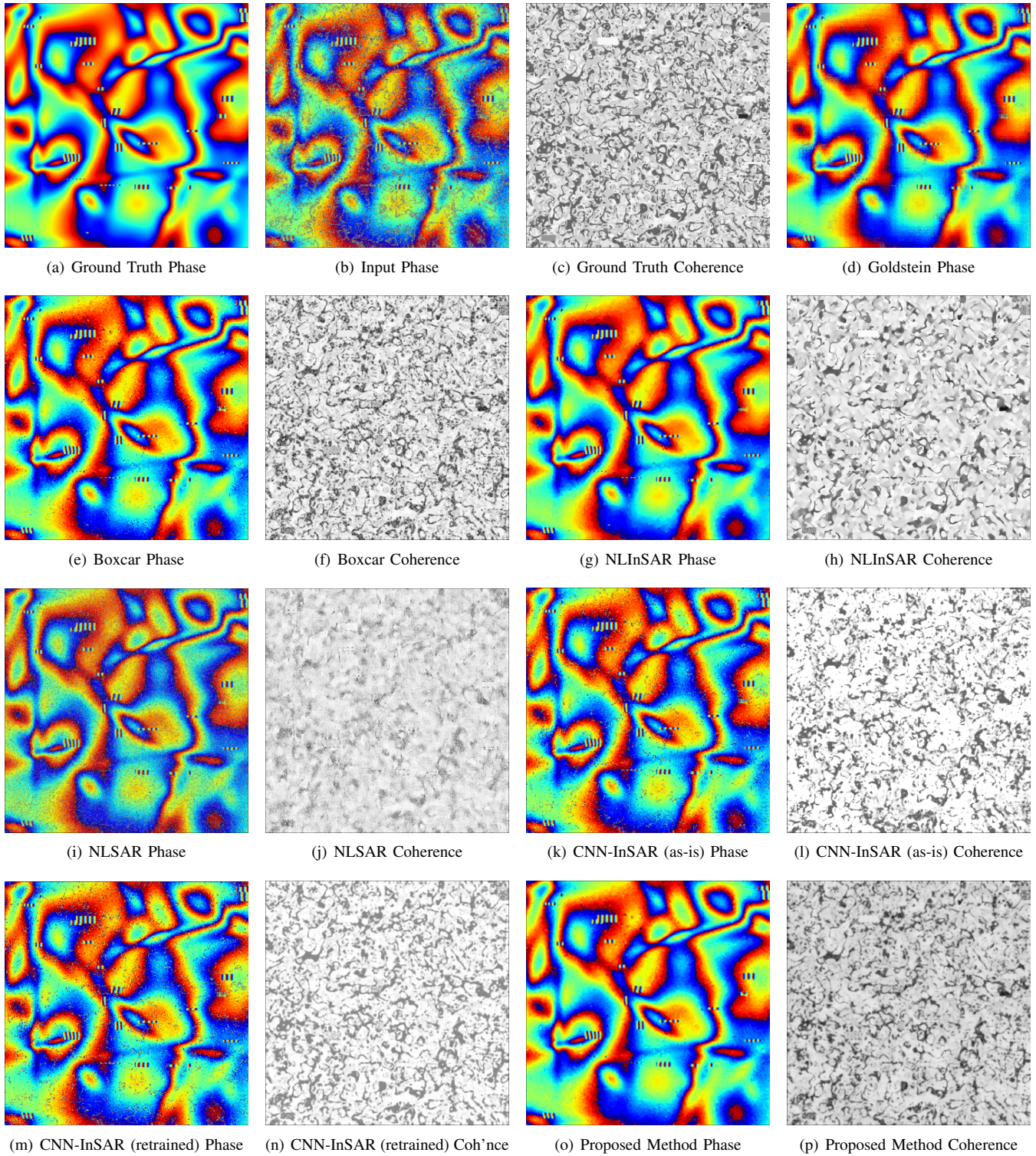


Fig. 4. Filtered phase and coherence outputs for simulated InSAR images processed by proposed and five existing methods. Visualizations for phase are coloured between  $-\pi$  (blue) to  $+\pi$  (red), and coherence between 0 (black: low) to 1 (white: high) respectively.

TABLE I

QUANTITATIVE EVALUATION OF PROPOSED AND EXISTING METHODS AND SCALABILITY OF PROPOSED METHOD OVER INCREASING GPU COUNTS

Method Name	Phase RMSE	Coherence RMSE	Residue Red. %	Cosine Error ( $\epsilon_{cos}^{\Delta\theta}$ )	Time (sec)		
CNN-InSAR (as-is)	1.270 ±0.191	0.257 ±0.013	92.74 ±3.30	0.060 ±0.036	1.42		
CNN-InSAR (retrained)	1.392 ±0.192	0.200 ±0.025	86.91 ±4.71	0.073 ±0.040	1.42		
NLSAR	1.537 ±0.073	0.301 ±0.055	35.85 ±17.71	0.132 ±0.012	11.49		
NLInSAR	0.850 ±0.122	0.159 ±0.018	97.59 ±2.08	0.014 ±0.009	20.44		
Goldstein	1.260 ±0.229	N/A	88.51 ±11.96	0.048 ±0.040	2.17		
Boxcar	1.025 ±0.173	0.143 ±0.018	97.64 ±1.94	0.025 ±0.021	1.32		
<b>Proposed (GenInSAR)</b>	<b>0.805 ±0.128</b>	<b>0.144 ±0.025</b>	<b>99.66 ±0.20</b>	<b>0.010 ±0.008</b>	<b>20.61</b>		
GPU Count	64	32	16	8	4	2	1
Time (sec)	0.38	0.65	1.35	2.44	5.11	9.38	20.61

[3] A. Mestre-Quereda, J. M. Lopez-Sanchez, J. Selva, and P. J. Gonzalez, "An improved phase filter for differential sar interferometry based on an iterative method," *IEEE Transactions on Geoscience and Remote Sensing*, vol. 56, no. 8, pp. 4477–4491, Aug 2018.

[4] A. Zimmer and P. Ghuman, "Cuda optimization of non-local means extended to wrapped gaussian distributions for interferometric phase denoising," *Procedia Computer Science*, vol. 80, pp. 166 – 177, 2016, international Conference on Computational Science 2016, ICCS 2016, 6-8 June 2016, San Diego, California, USA.

[5] X. Qing, J. Guowang, Z. Caiying, W. Zhengde, H. Yu, and Y. Peizhang, "The filtering and phase unwrapping of interferogram," in *Proceedings of International Society for Photogrammetry and Remote Sensing (ISPRS), Volume XXXV, Technical Commission VI/Working Group 4*, 2004.

[6] X. Lin and D. Niu, "Experiments of interferometric phase filtering through weighted nuclear norm minimization," in *Proceedings of the 2nd International Conference on Big Data Technologies*, ser. ICBTD2019. New York, NY, USA: ACM, 2019, pp. 278–282.

[7] J.-S. Lee, K. P. Papathanassiou, T. L. Ainsworth, M. R. Grunes, and A. Reigber, "A new technique for noise filtering of sar interferometric phase images," *IEEE Transactions on Geoscience and Remote Sensing*, vol. 36, no. 5, pp. 1456–1465, Sep. 1998.

[8] R. M. Goldstein and C. L. Werner, "Radar interferogram filtering for geophysical applications," *Geophysical Research Letters*, vol. 25, no. 21, pp. 4035–4038, 1998.

[9] N. Wu, D.-Z. Feng, and J. Li, "A locally adaptive filter of interferometric phase images," *IEEE Geoscience and Remote Sensing Letters*, vol. 3, no. 1, pp. 73–77, Jan 2006.

[10] S. Fu, X. Long, X. Yang, and Q. Yu, "Directionally adaptive filter for synthetic aperture radar interferometric phase images," *IEEE Transactions on Geoscience and Remote Sensing*, vol. 51, no. 1, pp. 552–559, Jan 2013.

[11] C. Chao, K. Chen, and J. Lee, "Refined filtering of interferometric phase from insar data," *IEEE Transactions on Geoscience and Remote Sensing*, vol. 51, no. 12, pp. 5315–5323, Dec 2013.

[12] G. Vasile, E. Trouve, J.-S. Lee, and V. Buzuloiu, "Intensity-driven adaptive-neighborhood technique for polarimetric and interferometric sar parameters estimation," *IEEE Transactions on Geoscience and Remote Sensing*, vol. 44, no. 6, pp. 1609–1621, June 2006.

[13] R. Song, H. Guo, G. Liu, Z. Perski, and J. Fan, "Improved goldstein sar interferogram filter based on empirical mode decomposition," *IEEE Geoscience and Remote Sensing Letters*, vol. 11, no. 2, pp. 399–403, Feb 2014.

[14] M. Jiang, X. Ding, Z. Li, X. Tian, W. Zhu, C. Wang, and B. Xu, "The improvement for baran phase filter derived from unbiased insar coherence," *IEEE Journal of Selected Topics in Applied Earth Observations and Remote Sensing*, vol. 7, no. 7, pp. 3002–3010, July 2014.

[15] C. Lopez-Martinez and X. Fabregas, "Modeling and reduction of sar interferometric phase noise in the wavelet domain," *IEEE Transactions on Geoscience and Remote Sensing*, vol. 40, no. 12, pp. 2553–2566, Dec 2002.

[16] Y. Bian and B. Mercer, "Interferometric sar phase filtering in the wavelet domain using simultaneous detection and estimation," *IEEE Transactions on Geoscience and Remote Sensing*, vol. 49, no. 4, pp. 1396–1416, April 2011.

[17] X. Zha, R. Fu, Z. Dai, and B. Liu, "Noise reduction in interferograms using the wavelet packet transform and wiener filtering," *IEEE Geoscience and Remote Sensing Letters*, vol. 5, no. 3, pp. 404–408, July 2008.

[18] Y. ong Gao, S. Zhang, K. Zhang, and S. Li, "Frequency domain filtering SAR interferometric phase noise using the amended matrix pencil model," *Computer Modeling in Engineering & Sciences*, vol. 119, no. 2, pp. 349–363, 2019.

[19] H. Huang and Q. Wang, "A method of filtering and unwrapping sar interferometric phase based on nonlinear phase model," *Progress In Electromagnetics Research*, vol. 144, pp. 67–78, 2014.

[20] Z. Suo, J. Zhang, M. Li, Q. Zhang, and C. Fang, "Improved insar phase noise filter in frequency domain," *IEEE Transactions on Geoscience and Remote Sensing*, vol. 54, no. 2, pp. 1185–1195, Feb 2016.

[21] A. Pepe, Y. Yang, M. Manzo, and R. Lanari, "Improved emcf-sbas processing chain based on advanced techniques for the noise-filtering and selection of small baseline multi-look dinsar interferograms," *IEEE Transactions on Geoscience and Remote Sensing*, vol. 53, no. 8, pp. 4394–4417, Aug 2015.

[22] N. Anantrasirichai, J. Biggs, F. Albino, and D. Bull, "A deep learning approach to detecting volcano deformation from satellite imagery using synthetic datasets," *Remote Sensing of Environment*, vol. 230, p. 111179, 2019.

[23] A. Krizhevsky, I. Sutskever, and G. E. Hinton, "Imagenet classification with deep convolutional neural networks," in *Advances in Neural Information Processing Systems 25*, F. Pereira, C. J. C. Burges, L. Bottou, and K. Q. Weinberger, Eds. Curran Associates, Inc., 2012, pp. 1097–1105.

[24] S. Mukherjee, A. Zimmer, N. K. Kottayil, X. Sun, P. Ghuman, and I. Cheng, "Cnn-based insar denoising and coherence metric," in *2018 IEEE SENSORS*, Oct 2018, pp. 1–4.

[25] S. Mukherjee, A. Zimmer, X. Sun, P. Ghuman, and I. Cheng, "Cnn-based insar coherence classification," in *2018 IEEE SENSORS*, Oct 2018, pp. 1–4.

[26] M. Herlihy and N. Shavit, *The Art of Multiprocessor Programming, Revised Reprint*. Morgan Kaufmann Publishers, 2012.

[27] C. Deledalle, L. Denis, and F. Tupin, "NI-insar: Nonlocal interferogram estimation," *IEEE Transactions on Geoscience and Remote Sensing*, vol. 49, no. 4, pp. 1441–1452, April 2011.

[28] C. Deledalle, L. Denis, F. Tupin, A. Reigber, and M. Jger, "NI-sar: A unified nonlocal framework for resolution-preserving (pol)(in)sar denoising," *IEEE Transactions on Geoscience and Remote Sensing*, vol. 53, no. 4, pp. 2021–2038, April 2015.

[29] G. Baier, C. Rossi, M. Lachaise, X. X. Zhu, and R. Bamler, "A nonlocal insar filter for high-resolution dem generation from tandem-x interferograms," *IEEE Transactions on Geoscience and Remote Sensing*, vol. 56, no. 11, pp. 6469–6483, Nov 2018.

[30] C. M. Bishop, "Mixture density networks," Aston University, Birmingham, United Kingdom, Tech. Rep. NCRG/94/004, February 1994.

[31] N. Srivastava, G. Hinton, A. Krizhevsky, I. Sutskever, and R. Salakhutdinov, "Dropout: A simple way to prevent neural networks from overfitting," *J. Mach. Learn. Res.*, vol. 15, no. 1, pp. 1929–1958, Jan. 2014.

[32] Y. Lecun, L. Bottou, Y. Bengio, and P. Haffner, "Gradient-based learning applied to document recognition," *Proceedings of the IEEE*, vol. 86, no. 11, pp. 2278–2324, Nov 1998.

[33] D. Clevert, T. Unterthiner, and S. Hochreiter, "Fast and accurate deep network learning by exponential linear units (elus)," in *4th International Conference on Learning Representations, ICLR 2016, San Juan, Puerto Rico, May 2-4, 2016, Conference Track Proceedings*, 2016.

[34] M. Sandler, A. Howard, M. Zhu, A. Zhmoginov, and L. Chen, "Mobilenetv2: Inverted residuals and linear bottlenecks," in *2018 IEEE/CVF Conference on Computer Vision and Pattern Recognition*, June 2018, pp. 4510–4520.

[35] D. P. Kingma and J. Ba, "Adam: A method for stochastic optimization," in *3rd International Conference on Learning Representations, ICLR 2015, San Diego, CA, USA, May 7-9, 2015, Conference Track Proceedings*, 2015.

[36] F. Chollet et al., "Keras," <https://keras.io>, 2015.

[37] C. Dnior and A. Pepe, "Comparative study of SAR interferometric phase filtering algorithms," in *Advanced Topics in Optoelectronics, Microelectronics, and Nanotechnologies IX*, M. Vladescu, R. D. Tamas, and I. Cristea, Eds., vol. 10977, International Society for Optics and Photonics. SPIE, 2018, pp. 611 – 620.

- [38] C. Shorten and T. M. Khoshgoftaar, "A survey on image data augmentation for deep learning," *Journal of Big Data*, vol. 6, no. 1, Jul. 2019.
- [39] G. Baier. Github - gbaier/despeckcl: A c++ library for insar denoising images using opencl. [Online]. Available: <https://github.com/gbaier/despeckCL>